Journal of Thermal Analysis and Calorimetry (2019) 138:47–56
https://doi.org/10.1007/s10973-019-08146-3

Effect of silicate modulus of water glass on the hydration of alkali-activated converter steel slag

Jianwei Sun[1] · Zhonghui Chen[1]

Received: 11 November 2018 / Accepted: 16 February 2019 / Published online: 2 March 2019

Abstract
Converter steel slag, currently underutilized crystalline metallurgical residue, was investigated for use as a precursor for alkali activation. Water glass solution with various moduli (0.5, 1.0, 1.5 and 2.0) was used at the same Na_2O dosage of 4% in order to investigate effect of modulus on hydration. Pure cement paste with the same ratio of water to binder was selected as the control sample. Results show that modulus has a significant impact on the hydration and mechanical strength development of alkali-activated steel slag. Similar to pure cement paste, alkali-activated steel slag paste has C–S–H gel and $Ca(OH)_2$ as its main hydration products. However, alkali-activated steel slag pastes have lower hydration heat and fewer amounts of hydration products. Additional silicate has a retarding effect on the hydration of steel slag. Hydration heat, $Ca(OH)_2$ contents and non-evaporable water contents reduce with increasing modulus. In addition, high silicate modulus fines the pore structure and improves compressive strength of the hardened paste.

Keywords Converter steel slag · Alkali activation · Hydration · Water glass · Modulus

Introduction

The development of new alternative cement has attracted considerable attention due to the improvement in environmental consciousness. Alkali-activated solid wastes prepared with alkaline activators and industrial by-products are potential and promising cementitious materials due to their good performances, such as low cost, energy saving, better fire resistance, encapsulation of radioactive substances, solidification of hazardous wastes and resource recycling [1, 2]. In general, the most commonly used alkaline activators are sodium and potassium-based solutions, including silicates, hydroxide, sulfate and carbonate [3]. Theoretically, any material composed of silicates or aluminosilicates could be activated. Intensive research work has been carried out in developing alkali-activated binders, which indicated that inorganic polymeric materials are formed at relatively low temperature (< 100 °C) yielding an amorphous and semi-crystalline three-dimensional polymeric structure [4, 5]. Two models are used to describe alkali-activated systems based on the chemical composition of starting materials. One is the high-calcium [Ca + Si] system, whose main reaction product is a type of hydrated calcium (aluminum) silicate gel (C–(A)–S–H) with a low Ca/Si ratio. It was also reported that Ca^{2+} in C–A–S–H could be replaced by Na^{+}, forming a C–(N)–A–S–H inner type gel. The other is the low-calcium [Al + Si] system, whose main reaction product is N–A–S–H type gel. The typical precursors for these two systems are blast furnace slag and metakaolin/fly ash, respectively. The activation of low-calcium materials generally needs higher concentration of activator than that of high-calcium system due to its lower activity [6–8]. Alkali activation could be considered as a promising technology for the transformation of aluminosilicate industrial wastes into construction materials.

Converter steel slag (SS) is a by-product from the steel-refining process in a conversion furnace. It accounts for about 15–20% of the crude steel output [8]. SS mainly consists of rich CaO (45–60%), SiO_2 (10–15%), Al_2O_3 (1–5%), Fe_2O_3 (3–9%), FeO (7–20%), P_2O_5 (1–4%) and MgO (3–13%) [8, 9]. Its chemical composition is similar to that of cement. According to the alkalinity calculation

✉ Jianwei Sun
tbp1600602045@student.cumtb.edu.cn

[1] School of Mechanics and Civil Engineering, China University of Mining and Technology, Beijing 100083, China

method proposed by Mason [$M = \omega(CaO)/\omega(SiO_2 + P_2O_5)$], SS could be divided into low alkalinity slag ($M < 1.8$), middle alkalinity slag ($M = 1.8$–2.5) and high alkalinity slag ($M > 2.5$). The common mineral phases of SS are tricalcium silicate(C_3S), dicalcium silicate(C_2S), dicalcium ferrite(C_2F), tetra calcium aluminoferrite (C_4AF), RO phase (FeO–MnO–MgO solid solution) and free CaO [10, 11]. The cementitious property of SS mainly owes to its calcium silicate minerals. In terms of hydraulic activity, the mineral phases of SS can be classified into four groups: olivine group ($M = 0.9$–1.4), merwinite group ($M = 1.4$–1.6), dicalcium silicate group ($M = 1.6$–2.4) and tricalcium silicate group ($M > 2.4$) [9–12].

Nowadays, SS is mainly used as pebbles in road construction and as a mixer to produce cement [8–11]. It can also be used in the fertilizer production and sewage treatment [10, 11]. Nonetheless, most SS is still left untreated. The massively deposited SS can occupy the farmland and pollute soil and groundwater. Two factors limit its large application in the concrete and cement as a kind of additive. On the one hand, both free CaO and MgO may result in soundness problem when SS is applied in cement or concrete. Free CaO comes from the addition of lime during the ladle processing. MgO is usually ascribed to the addition of dolomite and the refractory lining of the furnaces. The internal expansion caused by the formation of $Ca(OH)_2$ (CH) and $Mg(OH)_2$ at the late age might damage the microstructure of matrix and lead to volumetric instability. On the other hand, C_3S content in SS is lower than that in cement, and C_2S phase in SS is different from that in cement due to the lower cooling rate of SS. C_2S undergoes a series of polymorphic transformations during cooling, especially β-C_2S to γ-C_2S transformation at 490 °C. It is accompanied by a volume increase in approximately 12% and finally causes the slag to pulverize itself. Compared to β-C_2S in cement clinkers, γ-C_2S in SS is relatively inert and hard to react with water, which results in a much lower early activity of SS. However, γ-C_2S in SS is found to exhibit significant cementitious property when chemical activators are used. The sensitivity of the materials to activation depends on the phase composition and fineness of the slag and the type of activator used [7, 8]. Unlike generally studied blast furnace slag and fly ash/metakaolin with vitreous phase, SS is highly crystalline. Although alkali-activated material has been widely studied, there are only a few studies on the alkali activation of crystalline slag. Kriskova et al. had shown that the hydraulic behavior of crystalline slag is greatly modified after mechanical and chemical activation [13–15]. Shi et al. studied the properties of crystalline ladle slag and also found that this blending slag showed significant cementitious properties in the presence of alkaline activator. Moreover, they found that considerable compressive strengths can be achieved by mixing crystalline ladle slag with siliceous materials under autoclave curing at 175 °C for 4 h [16, 17].

Many studies have found that sodium silicate (water glass) is the best alkali activator due to its relatively low cost and availability. Moreover, compared to sodium hydroxide, water glass can provide extra silicate sources for the formation of gels. Some studies have investigated effects of silicate modulus on the hydration and strength of alkali-activated materials. Moruf et al. used SS/ultrafine palm oil fuel ash as raw materials to study influence of silicate modulus. They found increasing modulus positively affected homogeneity and structural units of hydration product due to the difference in Si–Al substitution [18]. Gao et al. studied alkali-activated granulated blast-furnace slag/class F fly ash blends, and they found that lowering activator modulus could significantly accelerate the early reaction but too high or too low modulus had detrimental impact on strength [19]. Maochieh Chi investigated the properties and microstructure of alkali-activated fly ash mortars. The higher modulus and Na_2O dosage were the better properties of the mortars achieved [20]. Zhenguo Shi et al. also studied effects of silicate modulus and alkali dosage on alkali–silica reaction (ASR) of alkali-activated granulated blast-furnace slag. The highest ASR expansion with an intermediate silicate modulus was observed. The effect of silicate modulus on ASR expansion was found to be governed by the pore solution alkalinity [21]. Darko Krizan et al. studied alkali-activated slag cement and found that the cumulative hydration heat increased with increasing modulus, but was still lower than that of Portland cement [22].

Silicate modulus and Na_2O dosage are two significant factors that influence the performances of alkali-activated materials. Previous studies found that water glass-activated SS could exhibit higher strengths than other activated SS at room temperatures. However, few reports exist about the influence of modulus and the dosage of Na_2O on the alkali activation of SS. Therefore, it is important to study the influence of modulus on hydration of water glass-activated SS, which plays an important role in exploring the reaction mechanism and guiding the engineering design of alkali-activated SS.

Experimental

Raw materials

P.I. 42.5 Portland cement conforming to Chinese National Standard GB175-2007 (equivalent to European CEM I 74 42.5) and SS were used. Table 1 presents the major chemical oxide compositions obtained by X-ray fluorescence (XRF) analysis. CaO forms the largest constituent in

Table 1 Chemical compositions of raw materials/%

	CaO	SiO_2	Al_2O_3	$Fe_2O_3^a$	MgO	P_2O_5	MnO	TiO_2	$Na_2O_{eq}^b$	LOI
SS	41.82	16.93	5.85	19.37	7.37	1.63	4.17	1.17	0.33	1.86
Cement	63.10	22.19	4.48	3.23	2.41	–	–	–	0.53	2.03

[a] $Fe_2O_3 = Fe_2O_3 + FeO$

[b] $Na_2O_{eq} = Na_2O + 0.658\ K_2O$

the slag. The CaO/SiO_2 ratio is 2.55, and the Al_2O_3/SiO_2 ratio is 0.33. The alkalinity of SS in this study is 2.25 (belonging to dicalcium silicate or middle alkalinity slag), which is preferable as a cementitious material. The mineralogical phases of SS determined by the X-ray diffraction (XRD) analysis are shown in Fig. 1, which were measured by a Cu X-ray tube with a step size of 0.02° and a 2θ range from 10° to 70°. As can be seen in Fig. 1, SS is highly crystalline and the major phase is γ-C_2S.

The specific surface areas of cement and SS are 342 and 624 $m^2\ kg^{-1}$, respectively. The specific surface area of SS is approximately two times larger than that of cement. The shape of the SS particles was observed by a scanning electron microscopy (SEM) using a FEI Quanta 200 instrument (as shown in Fig. 2a). The particles have angular and irregular shapes, and their sizes are highly variable. This is also evident from the grain-size distribution graph (in Fig. 2b) measured by a laser particle size analyzer (Mastersizer 2000). The continuity of the particle size distribution is very poor. There are more coarse and fine particles than middle particles. The D50 for SS and cement are found to be 6.3 and 17.3 μm, respectively. A commercial water glass with a modulus ratio (SiO_2/Na_2O molar ratio) equal to 3.12 (8.5% Na_2O, 26.5% SiO_2 and 65% H_2O by mass) was prepared as alkali activators.

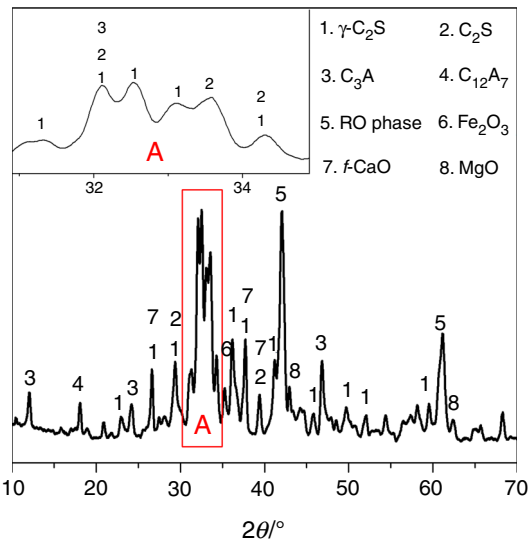

Fig. 1 XRD pattern of SS

NaOH (analytical reagent, 99 mass%) was used to adjust the modulus of sodium silicate solution.

Mix proportions

An equivalent Na_2O content of 4% by mass of SS and the water-to-binder ratio (W/B) of 0.45 were used in all mixes. The water consisted of the added distilled water and the water from activator solution. Four levels of activator moduli (0.5, 1.0, 1.5 and 2.0) were used. All solutions were first mixed to form aqueous solution of alkaline activator and cooled up to room temperature prior to further use. The detailed information of the mix proportions is listed in Table 2. Alkali-activated SS pastes (ASP) bars were prepared (40 mm × 40 mm × 40 mm). The pastes were mixed with distilled water, and a pure cement paste (PCP) was used as the reference sample (sample C-0.45). All samples were cured at 25 °C and > 90% RH until testing.

Testing methods

Compressive strength was measured as per Chinese standard GB177-85. In addition, the hydration kinetics of ASP was studied by an isothermal calorimeter (TAM Air, Thermometric) for the first 36 h under a constant temperature of 25 °C. The solid raw materials were firstly mixed with the activating solution for about 30 s, and then the paste was loaded into the calorimeter. The microstructure of the hardened paste was observed with SEM. The chemical compositions of hydration products were measured by energy-dispersive X-ray (EDX) analysis. Thermogravimetry (TG) curve was obtained by using a thermogravimetric analyzer Q5000 instrument with a heating rate of 10 °C/min from 50 to 900 °C in a through-flow N_2 atmosphere. The CH content of the paste was calculated based on the TG curve. The non-evaporable water content of the paste was obtained by the method of ignition loss. Autopore II 9220 mercury intrusion porosimeter (MIP) was applied to measure the pore structure of hardened pastes. The mass loss of samples was calculated between 50 and 1050 °C and then divided by the mass at 1050 °C. The results were corrected by the ignition loss of SS.

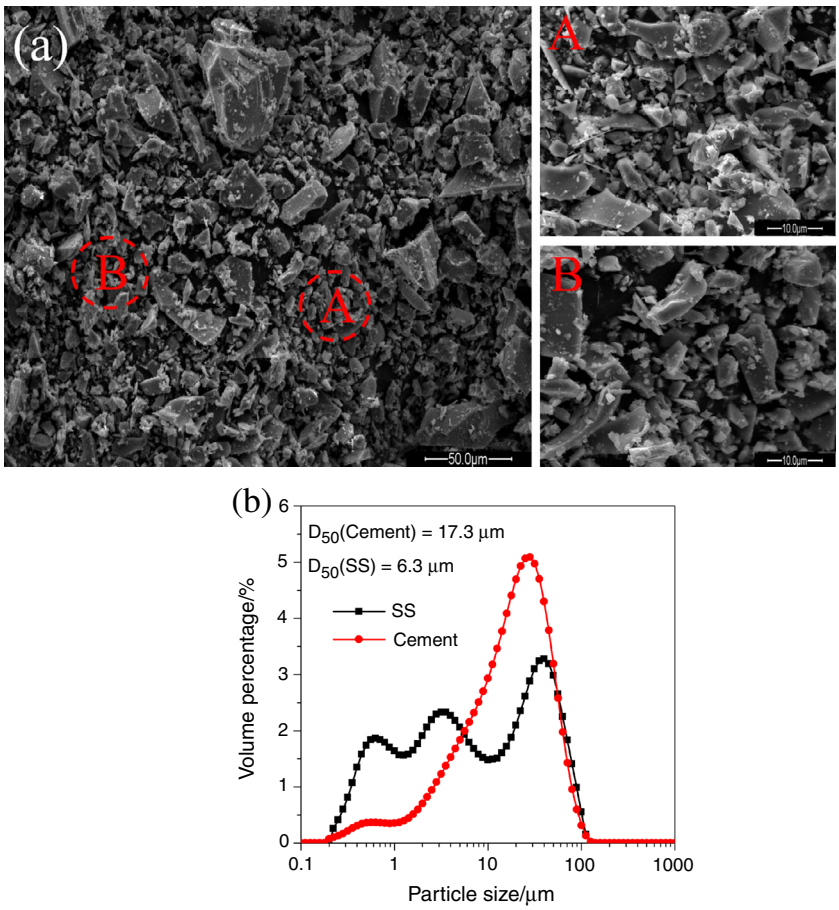

Fig. 2 **a** Angular particle morphology of SS. **b** Particle size distribution of raw materials

Table 2 Mix proportions of all mixes

Sample	Modulus	Binder	Mixing liquid	Na_2O/binder	W/B
C-0.45	–	Cement	Water	0	0.45
S-M0.5	0.5	SS	Water glass	4%	
S-M1.0	1.0				
S-M1.5	1.5				
S-M2.0	2.0				

Results and discussion

Heat of hydration

The isothermal calorimetric analyses per unit mass of the binders were conducted to all five mixes, and the results are illustrated in Fig. 3. In general, the hydration process of cement-based material can be divided into five stages: initial dissolution, induction/reorganization, acceleration, deceleration and stable period [1, 23]. Similar to exothermic rate curves of PCP, the ASP also has the typical five stages. However, ASP has a relatively higher, steeper and broader first peak than PCP. A very shorter induction period with higher hydration rate appears after first peak of ASP. Moreover, different from PCP, the shapes of second peaks of ASP are inconspicuous due to the different hydration mechanism between ASP and PCP. Calcium silicate and calcium aluminate in SS dissolve quickly due to high alkalinity from activator solution, forming the initial dissolved silicate and aluminate units. Finally, complexation reaction occurs with calcium and sodium, repolymerize to form gels and release heat. As can be seen in Fig. 3b, the cumulative hydration heat of ASP is higher than that of PCP before 9 h, whereas the heat is lower after 15 h due to slow rate of heat release after 9 h. The reason is that the amount of calcium silicate in SS is less than that in cement. Furthermore, the early hydration products formed by the rapid reaction wrap SS particles, which hinders the further reaction of SS. Therefore, ASP is "low-heat cement". This property plays a great role in massive concrete. And thermally induced stress cracks can be caused by a large temperature gradient [20–22].

During the second peak, the polymerization rate of initial reaction products exceeded the decomposition rate of SS. The number of monomers decreases as the reaction progresses. As can be seen in Fig. 3c, the acceleration period of ASP is significantly delayed and reaction rate of

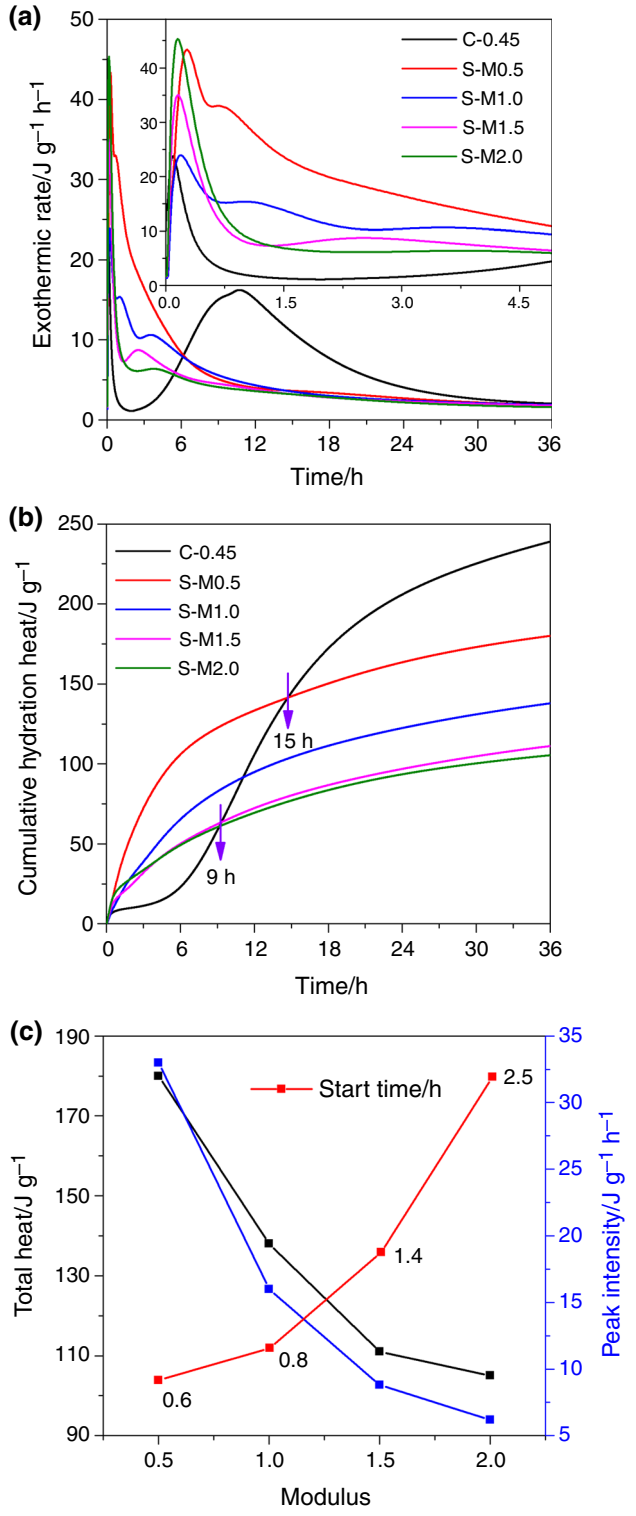

Fig. 3 Hydration heat evolution curves of all mixes at 25 °C. **a** Exothermic rate. **b** Cumulative hydration heat. **c** Start time, second peak intensity and total heat

second peak also drops as the modulus increases, which indicates that silicate has a retarding effect on the early reaction of ASP [24]. The cumulative hydration heats within 36 h are reduced with increasing modulus (in Fig. 3c), which illustrates reduction in total reaction products. This may be because the low alkalinity of the activator with high modulus results in little SS depolymerization and a slow reaction rate. Meanwhile, rich Ca^{2+} from SS reacts with abundant SiO_3^{2-} from the activator with higher modulus to form the highly amorphous silicate gel wrapping SS particles, which hinders the further reaction of SS.

The cumulative hydration heats of samples S-M1.5 and S-M2.0 are close to each other, suggesting that the presence of a higher level of silicate (modulus > 1.5) in the activator has a slight effect on reaction kinetics. The results of hydration heat seem different with the findings of other studies on blast furnace slag where it has been suggested that increased modulus results in increased reactivity [21, 22]. The probable reason is highly crystalline SS, but blast furnace slag has predominantly glassy phase. Compared to the highly crystalline material, the amorphous glassy phase with poor crystallinity is easily destroyed when exposed to the alkaline activator.

SEM and XRD analysis

SEM microphotographs and EDX point analyses spectrums of S-M0.5 at 3 days are given in Fig. 4. The SEM image and EDX spectrums clearly reflect the formation of product layers. It shows that SS particles are uniformly covered by a layer formed by the slag dissolution in alkali environment. The obvious presence of a big particle is RO phase (in Fig. 4, spot 1), which is difficult to dissolve. Some studies have shown that RO phase is undissolved crystal phase even though SS has hydrated for many years [11, 12]. A calcium silicate hydrate (C–S–H) gel is confirmed by EDX analysis (spot 2). Al substitution is low in C–S–H gel due to the low content in SS.

The XRD patterns of four ASPs with different moduli of activator are shown in Fig. 5. Compared to the pattern of SS, the intensities of some diffraction peaks remarkably decrease and some peaks disappear. It's clear that a wide diffraction peak nearby 29°–37° 2θ in curves appears, indicating that the amorphous three-dimensional network structure is formed. It is consistent with the conclusion of SEM observation. In addition, C_2S and C_3S crystallization diffraction peaks decrease, suggesting that they partially react with alkaline solution to produce two kinds of new hydrated products, C–S–H gel and CH. There is also $CaCO_3$ resulting from carbonization of CH.

TG analysis

TG is widely used to monitor the hydration process and determine the content of hydrated phases such as C–S–H

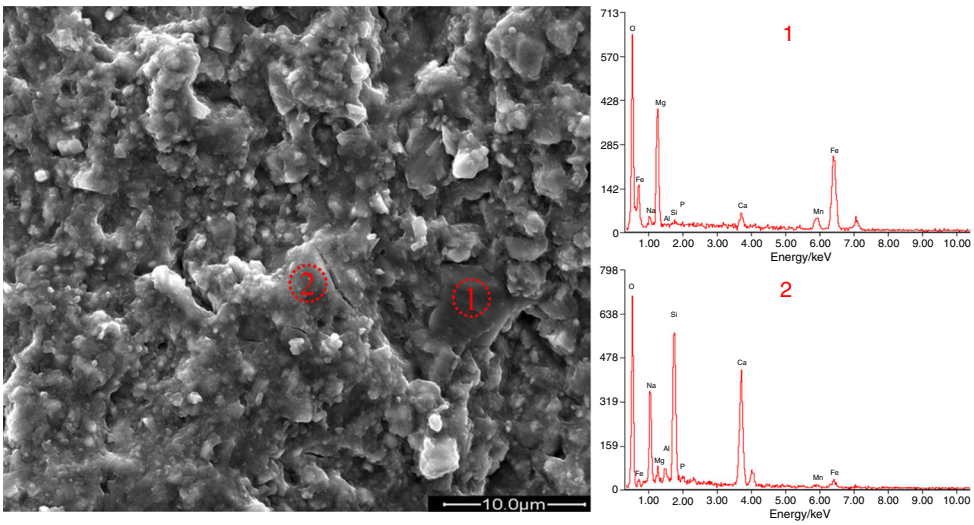

Fig. 4 SEM image and EDX spectrums of S-M0.5 at 3 days

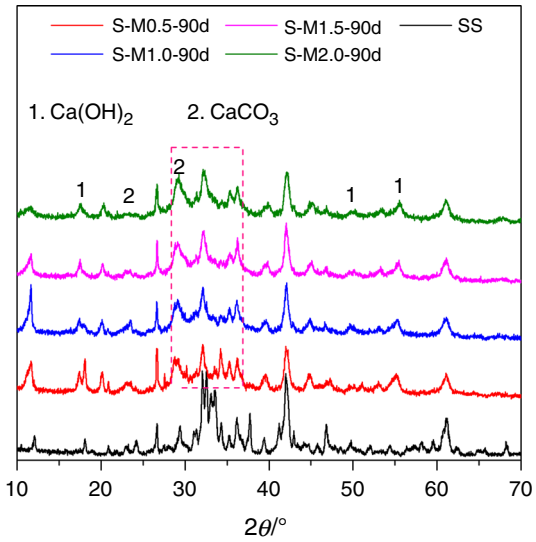

Fig. 5 XRD patterns of ASP at 90 days

and CH. Figure 6 shows TG curves of ASP and PCP. The detailed mass losses for all samples are signed. Both pastes experienced mass reductions with temperature increase. A mass reduction in ASP after temperature exposures is significantly lower than that of PCP at the same age. It states that the amount of hydration products of PCP is more than those of ASP, which is in line with the results of hydration heat. Exposure to high temperatures leads to changes in chemical structure and the dehydration of products. This is believed to be one of the reasons for the poorer performance of pure cement concrete after fire. In addition, a major mass loss of ASP occurs below 700 °C, suggesting that there is little decomposition of hydration products above 700 °C. This also provides evidence for better fire resistance of alkali-activated SS materials [25]. Obviously, the mass loss generally decreases as modulus increases. This phenomenon is more obvious in the early days (1 day and 3 days). It demonstrates that additional silicate has a retarding effect on the early reaction but a slight effect on the late hydration of ASP.

Mass loss usually corresponds to decomposition of substances. In general, there are three decomposition reactions in cement-based materials subjected to high temperature: the dehydration of C–S–H gel at around 100 °C, the decomposition of CH at around 400 °C and the decarbonization of $CaCO_3$ formed by carbonation reaction of CH at about 600 °C [26]. However, the decompositions of CH and $CaCO_3$ occur at lower temperature in ASP system than usual decomposition temperature. This might be due to the fact that the presence of alkali promotes the decomposition of carbonate phases [27]. The second possible reason can be that part of the carbonates formed is amorphous in nature. Indeed, these result in both poorly crystallized CH and $CaCO_3$ decompose at lower temperatures [27, 28]. Calculations were performed in accordance with the method proposed by Taylor [29], described in formula (1) for the dehydration of CH

$$W_{CH} = 74 \div 18 \times ML_{CH} + 74 \div 44 \times ML_{CaCO_3} \quad (1)$$

where ML_{CH} and ML_{CaCO_3} are mass loss during the dehydration of CH and the decomposition of $CaCO_3$, respectively. The molecular weights of CH, water and CO_2 are 74, 18 and 44, respectively. The CH contents of all samples are shown in Fig. 7. It is clear that the CH content in PCP is approximately two times more than that in ASP. CH is produced by the hydration of C_2S and C_3S. The total content of two minerals in SS is lower than that in cement, leading less CH in ASP. CH content of ASP decreases with increasing modulus, suggesting that the weaker alkalinity of the activator due to additional silicate inhibits the formation of CH.

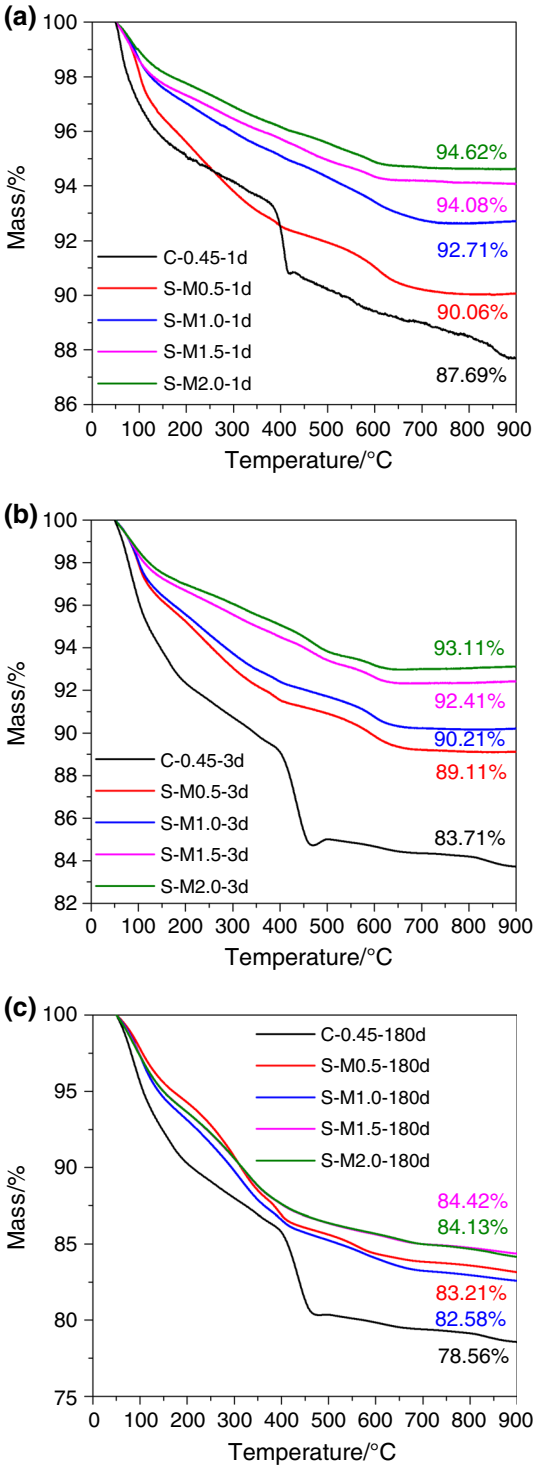

Fig. 6 TG analyses of all mixes. **a** 1 day. **b** 3 days. **c** 180 days

The non-evaporable water content

The non-evaporable water content is the important index of the hydration degree, which represents the relative amount of hydration products. The non-evaporable water content of the pastes at 1, 3 and 180 days is presented in Fig. 8. In

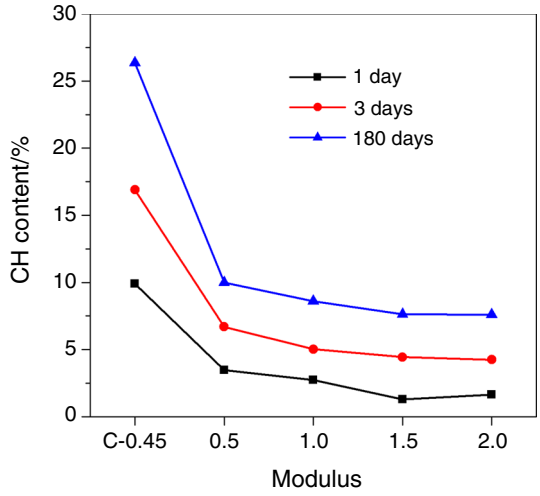

Fig. 7 CH contents of all mixes

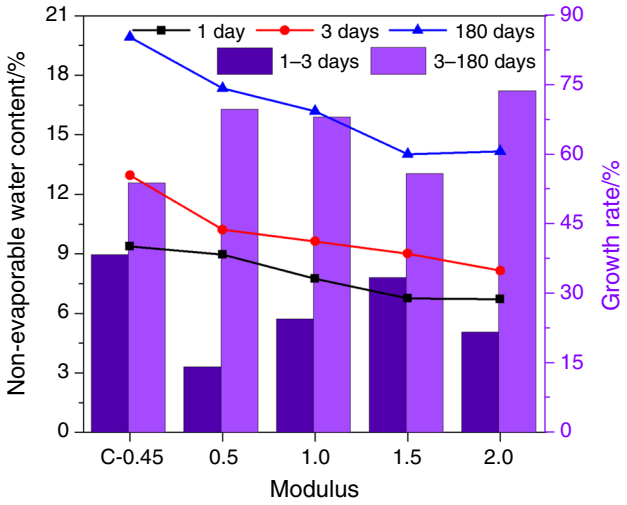

Fig. 8 Non-evaporable water content of the hardened pastes

line with the results of TG analysis, the non-evaporable water content, corresponding to hydration products, increases with the age of the samples, which indicates the enhancement of the hydration degree. As expected, the non-evaporable water content of ASP is smaller than that of PCP at all age, indicating that the hydration products of SS are much lower than that of cement. In ASP system, the non-evaporable water content generally decreases with increasing modulus, indicating that the increase in silicate can inhibit the hydration of SS. This phenomenon is more obvious in the early days (1 day and 3 days). However, the non-evaporable water contents of samples S-M1.5 and S-M2.0 at 180 days are very close to each other, indicating that the high modulus has little effect on the late-age (180 days) hydration degree of SS. The growth rate of ASP is lower from 1 to 3 days than that of PCP whereas is higher from 3 to 180 days. In other words, the later growth

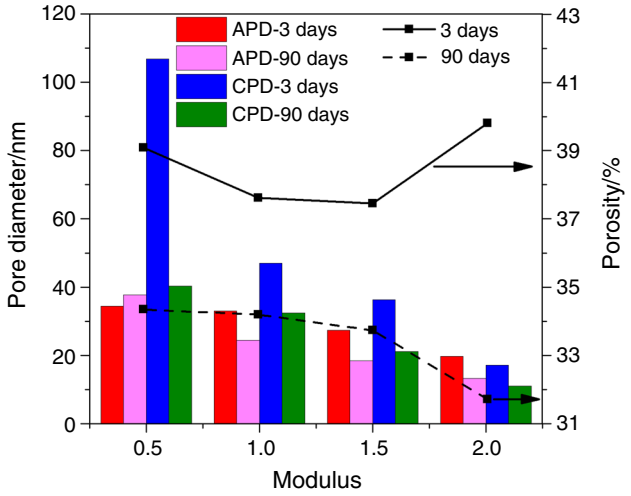

Fig. 9 Porosity, APD and CPD of all mixes

rate of ASP is far larger than that of PCP, which indicates larger growth of reaction degree of ASP.

Pore structure

Porosity, average pore diameter (APD) and critical pore diameter (CPD most probable pore diameter) of all pastes measured by MIP are shown in Fig. 9. According to the previous researches, the pores in cementitious materials are classified as follows: harmless pores (< 20 nm), little harmful pores (20–50 nm), harmful pores (50–200 nm) and much harmful pores (> 200 nm) [30, 31]. In this study, the pore structure distributions of different kinds of hardened pastes at the age of 3 days and 90 days are shown in Fig. 10.

As can be observed from Fig. 10, the cumulative pore volume and porosity decrease below modulus 1.5 at 3 days. Sample S-M2.0 has the highest pore volume and porosity. However, total volumes of harmless and little harmful pores significantly increase with the increase in modulus. The change of total harmful and much harmful pores volumes shows an obviously opposite trend. Meanwhile, APD and CPD decrease with the increase in modulus (in Fig. 9). The hydration degree of ASP continuously increased with ages. Compared to 3 days, the cumulative pore volume, porosity and APD and CPD obviously decrease at 90 days due to more hydration products filling the pores. In particular, sample S-M2.0 has the highest degree of reduction in porosity, from 39.8 to 31.7%. Similar to the tendency at 3 days, harmless pore volumes increase, but the total harmful and much harmful pores volumes decrease. This phenomenon suggests that increasing activator modulus can significantly reduce the pore size.

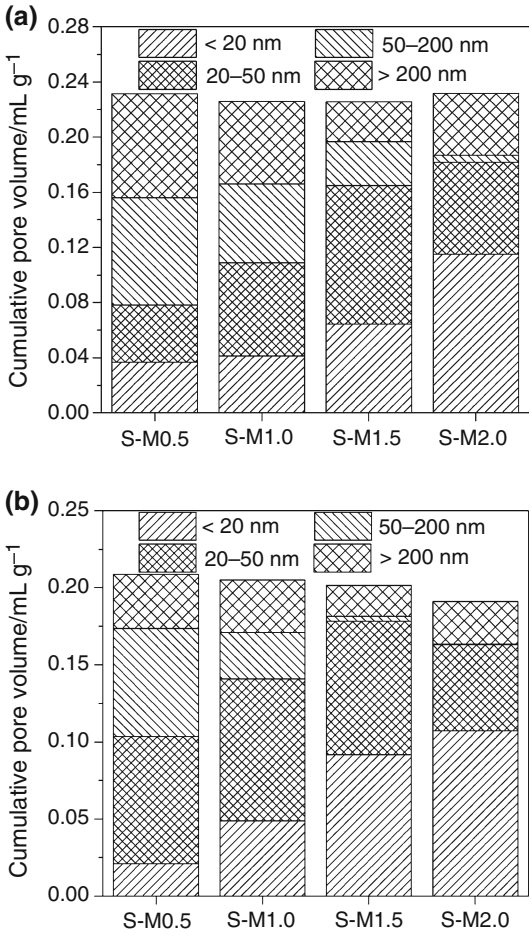

Fig. 10 Pore volume distribution. **a** 3 days. **b** 90 days

Compressive strength

The changes of compressive strength of all pastes with ages are shown in Fig. 11. As illustrated in Fig. 11, the compressive strengths of ASPs show similar tendency at all ages. Compressive strengths of ASPs relatively increase with the increase in modulus, which corresponds to the result of pore structure. Many researches have confirmed that the modulus of water glass has significant effect on the strength of the alkali-activated materials. At the same dosage of Na_2O, increasing modulus provides more silicate to the system for geopolymerization, thus improving the strength gains [32]. Moreover, Si/Al ratio is a significant parameter on the development of compressive strength. Additional silicate increases the Si/Al ratio resulting in more formation of Si–O–Si bonds, which are stronger than Si–O–Al and Al–O–Al bonds, thus leading to strength gain [33, 34]. Other studies suggested that the existence of more initial C–S–H and polymerization of SiO_3^{2-} in water glass solution with high modulus promotes formation of denser microstructure [21]. In this study, when the dosage is 4%, the optimum modulus for compressive strength is 2 for all

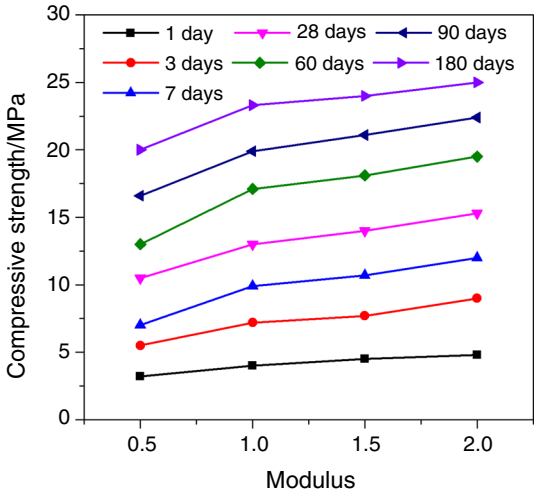

Fig. 11 Compressive strengths of ASP with different activator conditions

ages. However, in general, the pastes do not achieve appreciable compressive strength. The highest value is only 25 MPa at the age of 180 days. Therefore, SS as a sole precursor may not be an ideal raw material for alkali-activated cementitious material.

Conclusions

The alkali-activated SS cement, as low-cost product and with the possibility of using industrial waste, provides a solution to the present ecological problem. This study has investigated the influence of modulus of water glass on reaction degree, porosity and compressive strength of ASP at the same Na_2O content of 4%. The main conclusions extracted from this research are as follows:

1. Hydration processes of ASP and PCP are similar to each other. However, ASP has lower cumulative heat of hydration. Hydration heat of ASP reduces with the increase in modulus.
2. Similar to PCP, ASP also has C–S–H gel and CH as main hydration products. However, the amount of hydration products of SS activated by water glass is much less. CH content and non-evaporable water content decrease as modulus increases.
3. Total volumes of harmless and little harmful pores significantly increase with the increase in modulus. And total harmful and much harmful pores volumes reduce. It states that increasing activator modulus can significantly reduce pore size. Therefore, the higher the modulus of alkaline solution, the more superior the compressive strength of ASP. Furthermore, higher silicate modulus provides more and stronger Si–O–Si bonds, which also improves compressive strength.
4. Under the Na_2O dosage of 4% and water-to-binder ratio of 0.45, silicate modulus 2 may be considered as the optimum modulus based on the results.

Acknowledgements Authors acknowledge the support from the National Key Research and Development Program of China (2017YFC1503100).

Compliance with ethical standards

Conflict of interest The authors declare that they have no conflict of interest.

References

1. Sun J, Wang Z, Chen Z. Hydration mechanism of composite binders containing blast furnace ferronickel slag at different curing temperatures. J Therm Anal Calorim. 2018;131(3):2291–301.
2. Sun J, Chen Z. Influences of limestone powder on the resistance of concretes to the chloride ion penetration and sulfate attack. Powder Technol. 2018;338:725–33.
3. Wang D, Wang Q, Fang Z. Influence of alkali activators on the early hydration of cement–based binders under steam curing condition. J Therm Anal Calorim. 2017;130(1):1–16.
4. Tang SW, Yao Y, Li CAZJ. Recent durability studies on concrete structure. Cem Concr Res. 2015;78:143–54.
5. Ding Y, Dai JG, Shi CJ. Mechanical properties of alkali-activated concrete: a state-of-the-art review. Constr Build Mater. 2016;127:68–79.
6. Kani EN, Allahverdi A, Provis JL. Calorimetric study of geopolymer binders based on natural pozzolan. J Therm Anal Calorim. 2017;127(3):1–10.
7. Pacheco-Torgal F, Castro-Gomes J, Jalali S. Alkali-activated binders: a review: part 1. Historical background, terminology, reaction mechanisms and hydration products. Constr Build Mater. 2008;22(7):1305–14.
8. Pacheco-Torgal F, Castro-Gomes J, Jalali S. Alkali-activated binders: a review. Part 2. About materials and binders manufacture. Constr Build Mater. 2008;22(7):1315–22.
9. Wang Q, Yan P, Feng J. A discussion on improving hydration activity of steel slag by altering its mineral compositions. J Hazard Mater. 2011;186(2–3):1070–5.
10. Shi M, Wang Q, Zhou Z. Comparison of the properties between high-volume fly ash concrete and high-volume steel slag concrete under temperature matching curing condition. Constr Build Mater. 2015;98:649–55.
11. Wang Q, Shi M, Yang J. Influence of classified steel slag with particle sizes smaller than 20 μm on the properties of cement and concrete. Constr Build Mater. 2016;123:601–10.
12. Han F, Zhang Z. Properties of 5-year-old concrete containing steel slag powder. Powder Technol. 2018;334:27–35.
13. Kriskova L, Pontikes Y, Cizer Mertens G, Veulemans W, Geysen D, Jones PT, Vandewalle L, Van Balen K, Blanpain B. Effect of mechanical activation on the hydraulic properties of stainless steel slags. Cem Concr Res. 2012;42(6):778–88.
14. Kriskova L, Pontikes Y, Zhang F, Cizer Jones PT, Van Balen K, Blanpain B. Influence of mechanical and chemical activation on the hydraulic properties of gamma dicalcium silicate. Cem Concr Res. 2014;55(1):59–68.
15. Kriskova L, Pontikes Y, Cizer Malfliet A, Dijkmans J, Sels B, Van Balen K, Blanpain B. Hydraulic behavior of mechanically

and chemically activated synthetic merwinite. J Am Ceram Soc. 2014;97(12):3973–81.
16. Shi C. Characteristics and cementitious properties of ladle slag fines from steel production. Cem Concr Res. 2002;32:459–62.
17. Shi C, Hu S. Cementitious properties of ladle slag fines under autoclave curing conditions. Cem Concr Res. 2003;33(11):1851–6.
18. Yusuf MO, Johari MAM, Ahmad ZA. Impacts of silica modulus on the early strength of alkaline activated ground slag/ultrafine palm oil fuel ash based concrete. Mater Struct. 2015;48(3):733–41.
19. Gao X, Yu QL, Brouwers HJH. Reaction kinetics, gel character and strength of ambient temperature cured alkali activated slag–fly ash blends. Constr Build Mater. 2015;80:105–15.
20. Chi M. Effects of modulus ratio and dosage of alkali-activated solution on the properties and micro–structural characteristics of alkali-activated fly ash mortars. Constr Build Mater. 2015;99:128–36.
21. Shi Z, Shi C, Wan S. Effects of alkali dosage and silicate modulus on alkali–silica reaction in alkali-activated slag mortars. Cem Concr Res. 2018;111:104–15.
22. Krizan D, Zivanovic B. Effects of dosage and modulus of water glass on early hydration of alkali–slag cements. Cem Concr Res. 2002;32(8):1181–8.
23. Zhao J, Wang D, Yan P. Self-cementitious property of steel slag powder blended with gypsum. Constr Build Mater. 2016;113:835–42.
24. Gebregziabiher BS, Thomas RJ, Peethamparan S. Temperature and activator effect on early-age reaction kinetics of alkali-activated slag binders. Constr Build Mater. 2016;113:783–93.
25. Rashad AM, Bai Y, Basheer PAM. Chemical and mechanical stability of sodium sulfate activated slag after exposure to elevated temperature. Cem Concr Res. 2012;42(2):333–43.
26. Salman M, Cizer Ö, Pontikes Y. Alkali activation of AOD stainless steel slag under steam curing conditions. J Am Chem Soc. 2015;98(10):3062–74.
27. Salman M, Pontikes Y, Snellings R. Cementitious binders from activated stainless steel refining slag and the effect of alkali solutions. J Hazard Mater. 2015;286:211–9.
28. Wieczorek-ciurowa K, Paulik J, Paulik F. Influence of foreign materials upon the thermal decomposition of dolomite, calcite and magnesite part I. Influence of sodium chloride. Thermochim Acta. 1980;38:157–64.
29. Taylor H. Cement chemistry. 1st ed. London: Academic Press Limited; 1990.
30. Pang B, Zhou Z, Xu H. Utilization of carbonated and granulated steel slag aggregate in concrete. Constr Build Mater. 2015;84:454–67.
31. Nazari A, Riahi S. Microstructural, thermal, physical and mechanical behavior of the self-compacting concrete containing SiO_2 nanoparticles. Mater Sci Eng A. 2010;527(29):7663–72.
32. Nicolas RS, Bernal SA, Gutiérrez RMD. Distinctive microstructural features of aged sodium silicate-activated slag concretes. Cem Concr Res. 2014;65(11):41–51.
33. Leong HY, Ong DEL, Sanjayan JG. The effect of different Na_2O and K_2O ratios of alkali activator on compressive strength of fly ash based-geopolymer. Constr Build Mater. 2016;106:500–11.
34. Ryu GS, Lee YB, Koh KT. The mechanical properties of fly ash-based geopolymer concrete with alkaline activators. Constr Build Mater. 2013;47(5):409–18.